ACS OMEGA

http://pubs.acs.org/journal/acsodf

Article

Facile Synthesis and DFT Analysis of Novel Thiazole-Based Hydrazones: An Experimental and Theoretical Perspective

Muhammad Haroon, Tashfeen Akhtar,* Qurat-ul-ain Shaikh, Hasnain Mehmood, Muhammad Khalid,* Muhammad Adnan Asghar, Saad M. Alshehri, and Suvash Chandra Ojha*

Cite This: *ACS Omega* 2023, 8, 27488−27499

Read Online

ACCESS | Metrics & More | Article Recommendations | Supporting Information

ABSTRACT: Hydrazone compounds with remarkable nonlinear optical (NLO) properties were found with vast applications due to their cost-effective synthesis and greater stability. Therefore, we synthesized hydrazone scaffolds (**TCAH1**−**TCAH8**) by condensation reaction, and their structural confirmation was accomplished with spectroscopic methods (^{1}H-, ^{13}C-NMR, and HRMS). Quantum chemical calculations were also performed at B3PW91/6-311G(d,p) functional of DFT to explore electronic, structural, and chemical properties. To understand the NLO responses of afore-said chromophores, various kinds of analyses such as natural bonding orbitals (NBOs), frontier molecular orbitals (FMOs), UV−vis analysis, and density of states (DOS) were performed. Findings showed that the HOMO−LUMO energy gap in **TCAH8** (3.595 eV) was found to be lower than the **TCAH1**−**TCAH7** (4.123−3.932 eV) with a large red shift which leads to a substantial NLO response. Furthermore, strong intramolecular interactions showed the highest stabilization energy (24.1 kcal mol^{-1}) for **TCAH8** in the NBO transitions, combined with the least binding energy. The significant NLO response of **TCAH4** was explored with $\langle\alpha\rangle$, β_{tot}, and $\langle\gamma\rangle$ values as 5.157 × 10^{-23}, and 2.185 × 10^{-29}, and 2.753 × 10^{-34} esu, respectively, among the entitled compounds. The recent findings may inspire scientists to develop extremely effective NLO materials for forthcoming hi-tech applications.

INTRODUCTION

Nonlinear optical (NLO) materials found vast applications in the field of optical transmission, photonics, optoelectronics, electronics, and telecommunication.[1] To predict the physicochemical properties of a system, it is necessary to study its structure−property relationships (SPRs). For this purpose, density functional theory (DFT) has played a vital role.[2] It utilizes ab initio calculations to validate the molecular structures and interatomic potentials.[3] Moreover, DFT is used in quantum chemistry to determine electronic and photochemical characteristics.[4−6] Some other applications include their role in the formation of pharmacokinetic profiles for novel medications. Therefore, DFT is the method of choice to calculate the NLO properties of large electronic systems.[7] Hydrazones are an efficient class among the organic compounds and exhibit remarkable properties in the field of nonlinear optics. The hydrazone backbone strongly enhances the molecular nonlinearity via the strong push−pull mechanism of electron-donating and -withdrawing group substituents and performs a key role as an asymmetric electron transmitter.[8−10] Therefore, the researchers have been attracted toward these attributes of hydrazones to synthesize them as target NLO compounds. The first hyperpolarizability (β_{tot}) explained by the NLO analysis relates to ICT, taking place out of donor toward acceptor via π-conjugation. Therefore, structural variation of D−π−A organic compounds with diverse donor, acceptor, and π-bridge segments has been investigated earlier. Due to their extensive potential uses, the

Received: May 4, 2023
Accepted: July 10, 2023
Published: July 24, 2023

A−π−A framework has gained our interest to determine their nonlinear (NLO) characteristics.[11,12] It is anticipated that the π-conjugated acceptor groups lead to a sufficient push−pull force in the synthesized compounds, which could serve as an effective NLO material in several advanced technologies, such as optical communication, photovoltaic cells, organic light-emitting diodes, etc.[13]

This research work is based on the synthesis of new thiazole-hydrazone derivatives, namely, *N*′-((*E*)-benzylidene)-2-(2-((*E*)-benzylidene)hydrazineyl)thiazole-4-carbohydrazide (**TCAH1**), *N*′-((*E*)-2-chlorobenzylidene)-2-(2-((*E*)-2-chlorobenzylidene)hydrazineyl)thiazole-4-carbohydrazide (**TCAH2**), *N*′-((*E*)-3-chlorobenzylidene)-2-(2-((*E*)-3-chlorobenzylidene)hydrazineyl)thiazole-4-carbohydrazide (**TCAH3**), *N*′-((*E*)-4-chlorobenzylidene)-2-(2-((*E*)-4-chlorobenzylidene)hydrazineyl)thiazole-4-carbohydrazide (**TCAH4**), *N*′-((*E*)-2-bromobenzylidene)-2-(2-((*E*)-2-bromobenzylidene)hydrazineyl)thiazole-4-carbohydrazide (**TCAH5**), *N*′-((*E*)-3-methylbenzylidene)-2-(2-((*E*)-3-methylbenzylidene)hydrazineyl)thiazole-4-carbohydrazide (**TCAH6**), *N*′-((*E*)-4-methylbenzylidene)-2-(2-((*E*)-4-methylbenzylidene)hydrazineyl)thiazole-4-carbohydrazide (**TCAH7**), and *N*′-((*E*)-2-nitrobenzylidene)-2-(2-((*E*)-3-nitrobenzylidene)hydrazineyl)thiazole-4-carbohydrazide (**TCAH8**), and then exploration of NLO properties of these newly synthesized chromophores through DFT. From the literature, we found that such hydrazones and their NLO properties are not reported yet. The presence of π-conjugation in such compounds is stimulated by connecting the central core, i.e., 2-(*N*′-ethylidene-hydrazino)-thiazole-4-carboxylic acid ethylidene-hydrazide with different functional groups including electron-withdrawing and -donating moieties. To understand the NLO responses of afore-said chromophores, various kinds of analyses such as natural bonding orbitals (NBO), frontier molecular orbitals (FMOs), UV−vis analysis, and density of states (DOS) were performed. The configuration is divided into two fragments, where fragment 1 represents the π-bridge and fragment 2 represents two end-capped acceptors. Our study on the theoretical and experimental investigation of NLO compounds provides valuable insights into their structural, electronic, and optical properties. The comprehensive analysis presented here not only enhances our understanding of the fundamental principles governing NLO behavior but also opens up new avenues for the design and development of novel NLO materials. The insights gained from our work can aid experimentalists in the design and selection of promising candidates for further experimental characterization and application in optoelectronic devices.

RESULTS AND DISCUSSION

The compounds *N*′-(arylidene)-2-(2-arylidenehydrazinyl)-thiazole-4-carbohydrazides (**TCAH1−TCAH8**) were synthesized with simple condensation reaction with hydrazides and aryl aldehydes, as shown in Scheme 1. The reaction was carried out in the presence of acetic acid catalyst and methanol solvent. The products were obtained in good-to-excellent yield (65−98%).

The synthesized hydrazones were characterized by physical parameters (color, melting points, and retardation factor (R_f) values). The increase in melting point and R_f values are the initial parameters to authenticate their formation. Further authentication was achieved with ^{1}H-, ^{13}C-NMR, and HRMS techniques, and all spectra for synthesized compounds are listed in Figures S5−S28.

Scheme 1. Synthetic Pathway for *N*′-(Arylidene)-2-(2-(arylidene)hydrazinyl)thiazole-4-carbohydrazides (TCAH1−TCAH8)

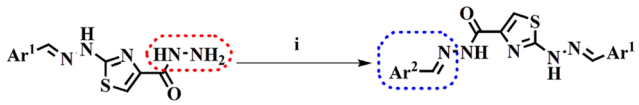

Compounds	Ar^1	Ar^2	Compounds	Ar^1	Ar^2
TCAH1	C_6H_5-	C_6H_5-	**TCAH2**	2-Cl-C_6H_4	2-Cl-C_6H_4
TCAH3	3-Cl-C_6H_4	3-Cl-C_6H_4	**TCAH4**	4-Cl-C_6H_4	4-Cl-C_6H_4
TCAH5	2-Br-C_6H_4	2-Br-C_6H_4	**TCAH6**	2-CH_3-C_6H_4	2-CH_3-C_6H_4
TCAH7	4-CH_3-C_6H_4	4-CH_3-C_6H_4	**TCAH8**	3-NO_2-C_6H_4	2-NO_2-C_6H_4

Reagents and conditions: i) Acetic acid, methanol, reflux 8-12 hours.

In ^{1}H-NMR, the appearance of a signal as a singlet for 1,3-thiazole ring C-5, −CH═N−, azomethine, −NH−N═, and −NH−CO− clearly justify our proposed structures. The proton of the thiazole ring was observed in the range of 7.51−8.10 ppm. The azomethine proton appeared in the range of 8.07−9.07 ppm. The proton of −NH−N═ functionality was indicated in the range of 11.24−11.86 ppm. The proton of NH−CO− group was identified in the range of 11.97−12.44 ppm. Most of the aromatic protons of **TCAH1**, **TCAH3**, **TCAH4**, **TCAH5**, and **TCAH6** were observed as multiplets. For compound **TCAH2**, two doublet of doublets of one proton each were observed at 7.92 (J = 2.41, 7.14 Hz) and 8.00 (J = 2.56, 6.75 Hz) ppm, respectively, indicating the presence of the *ortho* substitution at the aryl ring. The aromatic protons of **TCAH7** were observed as two doublets, each assigned for two protons in the range 7.55 (J = 6.63 Hz) and 7.59 (J = 6.97 Hz), respectively, justifying the presence of *para* substitution at the aryl ring. For compound **TCAH8**, aromatic protons were seen as doublet, triplet, and multiplet within the aromatic region.

The ^{13}C-NMR data showed aromatic carbons in the range of 116.4−142.9 ppm. The carbon signal in the range of 109.9−116.7 ppm was assigned to thiazole carbon at position 5 of the ring. The carbon signal appeared in the range of 140.4−148.5 ppm and was corroborated by thiazole carbon at position 4 of the ring. The −CH═N− and −CO−NH− carbons were indicated at 136.6−145.8 and 148.7−157.9 ppm, respectively. The most downfield carbon signal was assigned to thiazole carbon at position 2 of the ring at 168.3−168.9 ppm. Both proton and carbon signals helped in the correct interpretation of proposed structures.

The HRMS results of all synthesized **TCAHs** also supported our proposed structure. M + H^+, M + Na^+, and 2M + Na^+ peaks were observed for compounds **TCAH1**, **TCAH6**, and **TCAH7**. Compounds **TCAH3** and **TCAH4** possess only 2M + Na^+ peaks, and compounds **TCAH5** and **TCAH8** have only M + H^+ and M + Na^+ peaks, respectively. The compound **TCAH2** showed two M + H^+ and 2M + Na^+ peaks in HRMS. The results of HRMS are in good agreement with their calculated results.

Frontier Molecular Orbital Analysis. The frontier molecular orbital (FMO) investigation is a remarkable tool to explain chemical reactivity, stability, electronic properties, electron transport properties, and light-capturing potential of the molecules.[14] FMO contains two main orbitals: the highest occupied molecular orbital (HOMO) and the lowest unoccupied molecular orbital (LUMO).[15] Band gap is a

https://doi.org/10.1021/acsomega.3c03088
ACS Omega 2023, 8, 27488−27499

significant factor to explain hardness, softness, reactivity, and stability. A molecule with a small energy gap is considered as soft and reactive with greater polarizability as well as maximum charge transfer (ICT) and hence exhibits good NLO properties and vice versa.[16] Additionally, FMOs are crucial for developing the UV−vis spectrum as well as the analysis of the chemical reaction table. Keeping in view the importance of FMOs, herein, we calculated the E_{HOMO}, E_{LUMO}, and E_{gap} values for **TCAH1−TCAH8**, and their results are shown in Table 1.

Table 1. Computed FMO Energies and Their Energy Gap (ΔE) of Entitled Compounds in eV

compounds	E_{HOMO}	E_{LUMO}	ΔE (eV)
TCAH1	−5.757	−1.742	4.015
TCAH2	−5.992	−1.880	4.112
TCAH3	−6.104	−1.981	4.123
TCAH4	−5.923	−1.991	3.932
TCAH5	−5.865	−1.907	3.958
TCAH6	−5.689	−1.732	3.957
TCAH7	−5.634	−1.641	3.993
TCAH8	−6.162	−2.567	3.595

$\Delta E = E_{LUMO} - E_{HOMO}$; HOMO = highest occupied molecular orbital; LUMO = lowest unoccupied molecular orbital.

Data represented in Table 1 illustrated that band gaps vary by varying fragment 2 attached functional groups (−Cl, −Br, $-CH_3$, and $-NO_2$) on the terminal benzene ring. A literature survey reveals that compounds with high band gap require more energy to transfer electrons from the HOMO to the LUMO and compounds with low band gap require less energy to transfer electrons. The configuration in a series of hydrazone derivatives (**TCAH1−TCAH8**) is found to be A−π−A. Here, fragment 1 is kept rooted but fragment 2 is altered. The FMO study discloses that the maximum value of E_{gap} is observed in the **TCAH3** molecule, which is 4.123 eV, whereas **TCAH8** showed the minimum E_{gap} value of 3.595 eV. Overall, the declining order of E_{gap} is as follows: **TCAH3** > **TCAH2** > **TCAH1** > **TCAH7** > **TCAH5** > **TCAH6** > **TCAH4** > **TCAH8**. By incorporating the chloro group at the *meta* position, the maximum value of E_{gap} is observed in the **TCAH3** molecule, which is 4.123 eV as chloro is an electron-donating group due to a resonance effect and less withdrawal due to an inductive effect here, the resonance effect overcomes the inductive effect and it activates the ring and diminishes the charge transference from fragment 1 to fragment 2. The delocalization of electrons is not facilitating the flow of electrons out of the ring due to *meta* position of the substituent. Band gap is further reduced in **TCAH2** by substituting the chloro group at the *ortho* position on benzene which deactivates the ring at the *ortho* position; here, the inductive effect dominates the resonance effect of chloro as compared to at the *meta* position. The observed band gap is 4.112 eV. Charge transference is improved in **TCAH1** by incorporating benzene as fragment 2 and the band gap is reduced to 4.015 eV due to a strong withdrawing effect of the benzene group compared to the chloro group. Reduction in energy gap is observed in **TCAH7** by substituting the methyl group at *para* position, which donates the electrons to the benzene ring and activates the ring due to the resonance effect, and charge transference is improved. By incorporating the bromo group at the *ortho* position in **TCAH5**, charge is effectively transferred from fragment 1 to fragment 2 as bromo is *ortho para* directors on the ring, which is expected a decrease in the band gap due to possible conjugate with the second fragment as part of delocalization. The band gap is further reduced to 3.957 eV in **TCAH6** due to the methyl group at the *ortho* position. The band gap is reduced to a large extent by incorporating the chloro group at *para* position on benzene in **TCAH4** due to its strong withdrawing effect as an acceptor and deactivates the ring, and the charge is efficiently transferred from fragment 1 to fragment 2 which might be due to the resonance effect as it dominates over inductive and when it dominates then the transfer of electrons will take place over the whole conjugated unit. Furthermore, with the increase in distance, the inductive effect decreases, so in this case, the inductive effect cannot facilitate the electron transfer from the ring to fragment 2. By substituting strong electron-withdrawing nitro benzene as an acceptor unit, in **TCAH8**, the band gap remarkably reduced to 3.595 eV due to its strong withdrawing effect by means of both resonance and inductive effects, which deactivates the ring and charge transference is improved to a large extent. The contour surface for electron density distribution of FMOs effectively describes efficient ICT and is shown in Figure 1. For the HOMO, the charge densities are concentrated mainly at fragment 1 to fragment 2, while in **TCAH6** and **TCAH7**, it lies over the entire molecules. However, for the LUMO, it is located largely at the accepter moiety and partially over the spacer. In the case of **TCAH8**, it resides completely over fragment 2. As a result, the concerned compounds experience significant charge transfer toward fragment 2 (LUMO) from fragment 1. All synthetic compounds can be used as effective NLO materials mainly due to the assistance of charge transfer.

Global Reactivity Parameters (GRPs). The HOMO and LUMO are considered a crucial factor in determining compound's kinetic stability and chemical reactivity by assessing their global reactivity parameters.[17] They include electronegativity (X),[18] ionization potential (IP),[19] electron affinity (EA),[20] global softness (σ),[21] hardness (η),[22] chemical potential (μ),[23] and electrophilicity index (ω).[24] The outcomes for **TCAH1−TCAH8** are presented in Table 2.

According to Koopman's theorem, the electron affinity (A) and ionization potential (I) of the examined chromophores are used to describe the ability of HOMOs and LUMOs to donate and accept electrons, respectively. Additionally, I and A associated with **TCAH1−TCAH8** can be calculated as negative of their E_{HOMO} and E_{LUMO} values, respectively. I values depict the energy required to remove an electron from the valence band (HOMO). The literature study reveals that compounds with higher I values exhibit greater stability, resulting in chemical inertness.[25] I values of **TCAH1−TCAH8** are larger in magnitude than their corresponding A values, demonstrating the remarkable electron-donating capacity of the produced NLO molecules. The synthesized chromophore **TCAH8** has the greatest value of I (6.162 eV), indicating that it is difficult to transfer electron charge density to fragment 2, while **TCAH7** has the lowest I value of 5.634 eV. The ascending order of I is observed to be as follows: **TCAH7** < **TCAH6** < **TCAH1** < **TCAH5** < **TCAH4** < **TCAH2** < **TCAH3** < **TCAH8**.

Electronegativity (X) represents the ability of a molecule to attract the upcoming electrons toward itself. It is related to the chemical potential (μ) with negative values, which displays that the molecules are stable. Similarly, the parameters such as

https://doi.org/10.1021/acsomega.3c03088
ACS Omega 2023, 8, 27488−27499

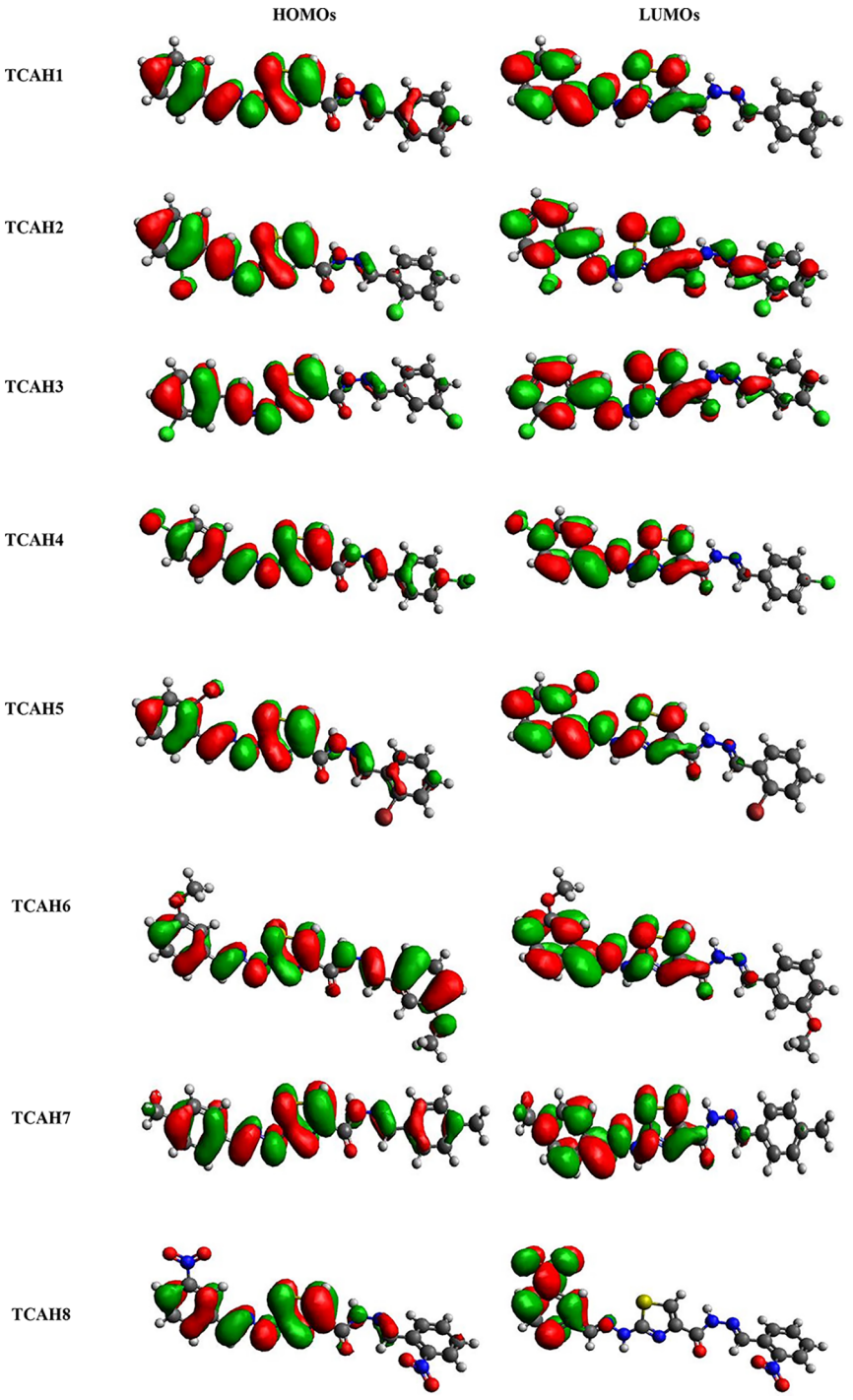

Figure 1. Frontier molecular orbitals (HOMO/LUMO) of the entitled compounds (**TCAH1−TCAH8**).

Table 2. GRP Values of Synthesized Compounds (TCAH1−TCAH8) in eV

compounds	I	A	X	η	μ	ω	σ	ΔN_{max}
TCAH1	5.757	1.742	3.749	4.015	−3.749	1.750	0.249	0.9337
TCAH2	5.992	1.880	3.936	4.112	−3.936	1.884	0.243	0.9572
TCAH3	6.104	1.981	4.043	4.123	−4.043	1.982	0.243	0.9806
TCAH4	5.923	1.991	3.957	3.932	−3.957	1.991	0.254	1.006
TCAH5	5.865	1.907	3.886	3.958	−3.886	1.908	0.253	0.9818
TCAH6	5.689	1.732	3.711	3.957	−3.711	1.740	0.253	0.9378
TCAH7	5.634	1.641	3.638	3.993	−3.638	1.657	0.250	0.9111
TCAH8	6.162	2.567	4.365	3.595	−4.365	2.650	0.278	1.214

https://doi.org/10.1021/acsomega.3c03088
ACS Omega 2023, 8, 27488−27499

global softness (σ) and hardness (η) of the compound give details about their reactivity. The highest η value obtained is 4.123 eV exhibited by **TCAH3**, which decreases to 3.932 eV in **TCAH4**. The lowest value of hardness, i.e., 3.595 eV is observed in **TCAH8**. The overall descending order of η is found to be **TCAH3** > **TCAH2** > **TCAH1** > **TCAH7** > **TCAH5** > **TCAH6** > **TCAH4** > **TCAH8**. The good correlation between this order and E_{gap} is an evidence that molecules with higher E_{gap} values are thought to be hard molecules with superior kinetic stability, less reactivity, and resistance to change in electronic configurations.[26] Likewise, the uppermost value of σ is exhibited by **TCAH8** (0.278 eV^{-1}), and the lowermost value of σ is observed in two designed compounds **TCAH3** and **TCAH2** as 0.243 eV^{-1}. Therefore, the overall ascending order of global softness is **TCAH3** = **TCAH2** < **TCAH1** < **TCAH7** < **TCAH5** = **TCAH6** < **TCAH4** < **TCAH8**, that is opposite to the increasing E_{gap} order.

Concluding the entire discussion it may be summed up that global reactivity descriptors and HOMO−LUMO band gap order have a strong correlation. Low-lying HOMO−LUMO gaps are widely recognized to improve the NLO response potentially. This statement is valid for the systems we studied, which provide promising potential for the possible use of the compounds under investigation due to their robust NLO responses in optoelectronic applications.

UV−Visible Analysis. To understand the excitations as well as absorption properties of the entitled compounds (**TCAH1−TCAH8**), their UV−vis analysis is accomplished by using the time-dependent density functional theory (TDDFT) with dichloromethane (DCM). The excitation energies (E), oscillator strengths (f_{os}), absorption wavelengths (λ_{max}), and molecular orbital (MO) contributions for synthesized compounds are presented in Table 3. The UV−vis spectra of compounds are shown in Figure 2, while the supplementary information is also provided in Tables S2−S9. The data have clearly elucidated that maximum absorption wavelengths (λ_{max}) and transition energy (E) findings are inversely related to each other.[27] The absorption maximum value drops as the transition energy of the compound increases. All the synthesized compounds **TCAH1−TCAH8** cover the absorption range from 318.0 to 342.9 nm. It can be observed that by substituting fragment 2, λ_{max} is greatly influenced and a bathochromic shift is observed. The least value of λ_{max} is observed as 318.0 nm in **TCAH3** along with 3.898 eV and a decline in charge transference is observed. Furthermore, it is analyzed that the band gap decreased to an extent by substituting chloro at the *ortho* position in **TCAH2** results an increase in conjugation due to the resonating effect, so absorbance increases to 321.1 nm with 3.861 eV. **TCAH6** and **TCAH1** are detected to be greater in absorption compared to **TCAH3** and **TCAH2** and observed λ_{max} are 331.4 and 333.2 nm, respectively, due to conjugation, and better charge transference from fragment 1 to fragment 2. By incorporating bromo and methyl groups in **TCAH5** and **TCAH7**, charge is effectively transferred from the HOMO to the LUMO and observed λ_{max} are 340.0 and 335.0 nm with corresponding energies of 3.646 and 3.701 eV, respectively, due to better charge transference from π-spacer to the acceptor. The band gap is reduced to a greater extent in **TCAH4** by substitution of the chloro group at *para* position and its withdrawing effect facilitates conjugation, stabilizes the electron density, and the charge is effectively transferred from the HOMO to the LUMO, and the observed band gap is 340.4 nm along with 3.642 eV. The synthesized compound **TCAH8** exhibits the highest absorption peak at 342.9 nm with 3.615 eV transition energy due to the strong withdrawing effect and extended conjugation facilitated by the nitro group, which enhances the push−pull effect from fragment 1 to fragment 2. Overall, the entitled compounds have shown the absorbance in the UV−vis region with the following decreasing order: **TCAH8** > **TCAH4** > **TCAH5** > **TCAH7** > **TCAH1** > **TCAH6** > **TCAH2** > **TCAH3**.

Table 3. Computed Transition Energies (E) in eV, Maximum Absorption Wavelengths (λ_{max}), Oscillator Strengths (f_{os}), and Major Contributions of TCAH1−TCAH8

compounds	DFT λ (nm)	E (eV)	f_{os}	major MO contributions (%)
TCAH1	333.2	3.721	0.705	H → L (97%)
TCAH2	321.1	3.861	0.922	H → L+1 (91%)
TCAH3	318.0	3.898	0.737	H → L+1 (95%)
TCAH4	340.4	3.642	0.882	H → L (96%)
TCAH5	340.0	3.646	0.746	H → L (95%)
TCAH6	331.4	3.741	0.794	H−1 → L (90%)
TCAH7	335.0	3.701	0.777	H → L (97%)
TCAH8	342.9	3.615	0.785	H → L+2 (70%)

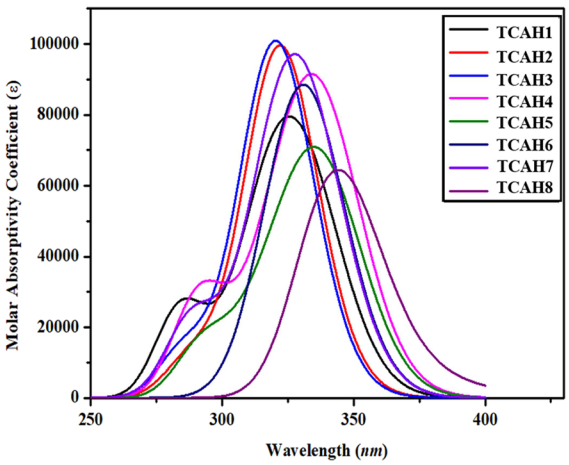

Figure 2. Simulated absorption spectra of the studied compounds (**TCAH1−TCAH8**).

The highest HOMO−LUMO electronic transitions are recorded as 97% in **TCAH1** and **TCAH7** compounds and occur from H → L. The least contribution obtained is 70% due to H → L+2 in **TCAH8**. The other compounds **TCAH3**, **TCAH2**, **TCAH5**, **TCAH6**, **TCAH4**, and **TCAH7** have shown the contributions between these percentages, as shown in Table 3. Thus, it is obvious that the functional groups substitution in the acceptor group in all tailored compounds successfully increased the absorption wavelength in the synthesized derivatives. The **TCAH8** derivative shows the highest bathochromic shift (342.9 nm), which is expected to be a somewhat promising novel NLO compound.

Natural Bond Orbital Analysis. Natural bond orbital (NBO) analysis is used to study the conjugative interactions between fragment 1 and fragment 2 groups, hyper conjugative interactions, and intramolecular charge transfer (ICT).[28] One of the significant aspects of NBO analysis is that it analyzes the

https://doi.org/10.1021/acsomega.3c03088
ACS Omega 2023, 8, 27488−27499

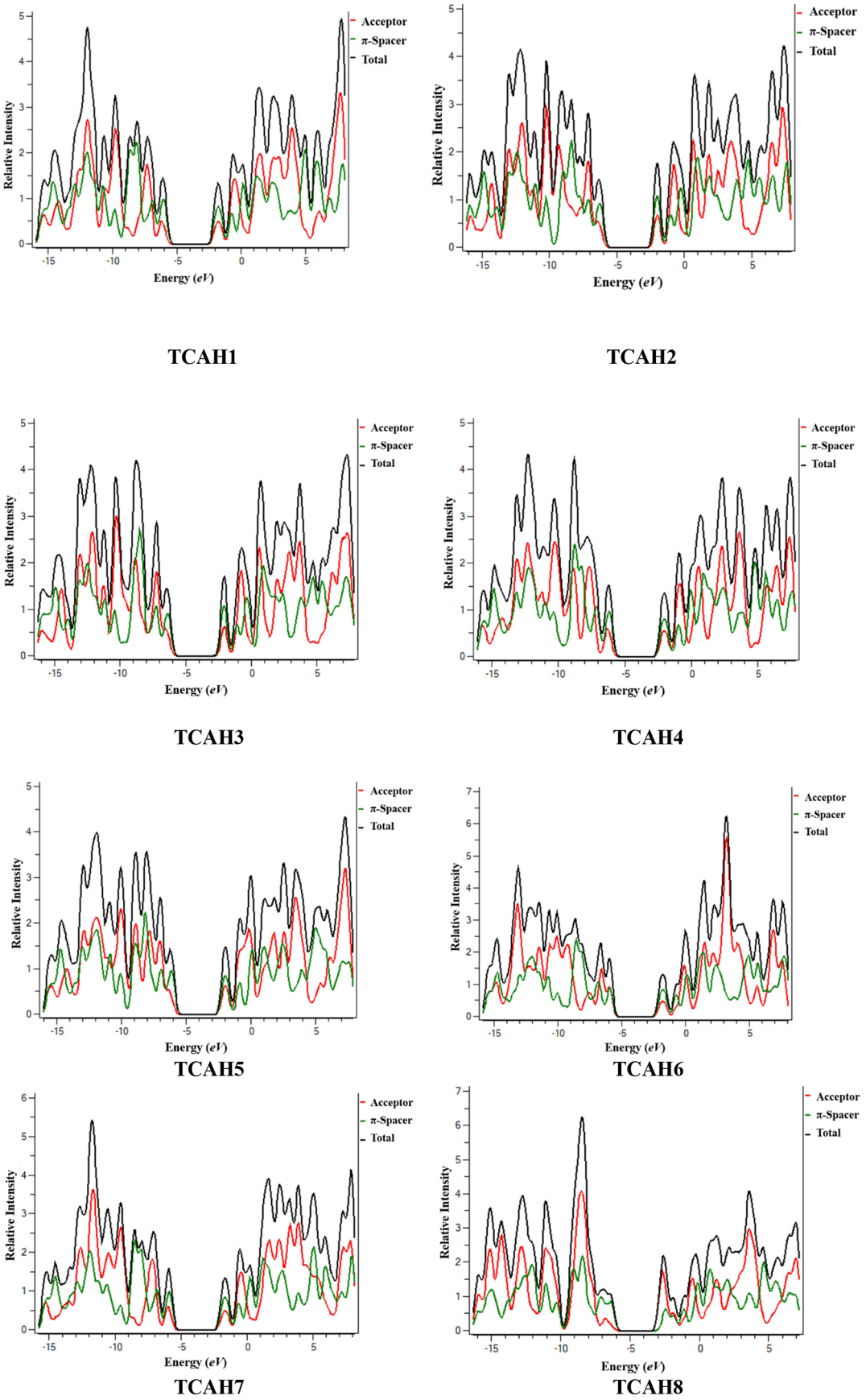

Figure 3. Density of states pictographs for the synthesized compounds.

https://doi.org/10.1021/acsomega.3c03088
ACS Omega 2023, 8, 27488−27499

delocalization of electronic charges, and the charge density transfers from fragment 1 to the fragment 2 region of the system with the A−π−A architecture. The second-order Fock matrix is employed to calculate several types of interactions and their stabilization energies on the NBO basis.[29]

Major findings from the **TCAH1−TCAH8** systems' NBO investigation are shown in Table S18. The supplemental information contains a thorough NBO analysis (see Tables S10−S17).

Mostly four types of transitions, i.e., $\pi \rightarrow \pi^*$, $\sigma \rightarrow \sigma^*$, LP → π^*, and LP → σ^* are studied in an organic system. Among all of them, the most dominant transitions are $\pi \rightarrow \pi^*$, which occur due to π-conjugation in a chromophore. The $\sigma \rightarrow \sigma^*$ transitions are weak electronic transitions as compared to all other types and occur due to the excitation of electrons occupying a HOMO of a sigma bond toward the LUMO of that bond.

In **TCAH1−TCAH8**, the higher stabilization energies obtained through $\pi \rightarrow \pi^*$ transitions are found as 21, 22.23, 22.16, 22.14, 21.27, 22.54, 22.41, and 24.1 kcal/mol for π(C20−C22) → π^*(C21−C24), (C3−N6) → π^*(C1−C2), π(C3−N6) → π^*(C1−C2), π(C18−C19) → π^*(C21−C24), π(C20−C22) → π^*(C21−C24), π(C18−C20) → π^*(C22−C24), π(C29−C32) → π^*(C26−C27), and π(C22−C24) → π^*(C19−C21) transitions, respectively. Similarly, the least energy values: 0.61, 0.56, 0.58, 0.6, 0.56, 0.57, 0.56, and 0.53 kcal/mol are observed for π(C1−C2) → π^*(C8−O9), π(C9−O10) → π^*(C9−O10), π(C9−O10) → π^*(C9−O10), π(C8−9) → π^*(C8−O9), π(C8−O9) → π^*(C8−−O9), π(C28−C31) → π^*(C28−C31), π(N13−C16) → π^*(N13−C16), and (C8−O9) → π^*(C8−O9), correspondingly. Moreover, the higher value of stability due to weak interactions such as $\sigma \rightarrow \sigma^*$ transition is noted for σ(C2−N6) → σ^*(C3−N7), σ(N7−H8) → σ^*(C3−S4), σ(N13−C15) → σ^*(N7−N13), σ(C2−N6) → σ^*(C3−N7), σ(C2−N6) → σ^*(C3−N7), σ(C2−N6) → σ^*(C3−N7), σ (C2−N6) → σ^*(C3−N7), and σ(C2−N6) → σ^*(C3−N7) with stabilization energies as 7.14, 6.78, 6.71, 7.15, 7.14, 7.14, 7.14, and 7.17 kcal/mol, respectively. The lower value of stability due to strong interactions such as $\sigma \rightarrow \sigma^*$ transition is noted for σ(C1−H5) → σ^*(C3−S4), σ(C15−H16) → σ^*(C15−C28), σ(N7−H8) → σ^*(C3−S4), σ(C1−H5) → σ^*(C3−S4), σ(C1−H5) → σ^*(C3−S4), σ(C3−N7) → σ^*(N7−H34), σ(C3−N7) → σ^*(N7−H38), and σ(C1−H5) → σ^*(C3−S4) with stabilization energies as 0.5, 0.51, 0.5, 0.51, 0.51, 0.5, 0.5, and 0.51 kcal/mol, respectively.

In **TCAH1−TCAH8**, the higher stabilization energy is obtained through LP1 → π^* transition and noted for LP1(N10) → π^*(C8−O9), LP1(N11) → π^*(C9−O10), LP1(N11) → π^*(C9−O10), LP1(N10) → π^*(C8−O9), LP1(N10) → π^*(C8−O9), LP1(N10) → π^*(C8−O9), (N10) → π^*(C8−O9), and LP1(N10) → π^*(C8−O9) with stabilization energies as 52.81, 51.78, 52.36, 52.5, 51.54, 53.05, 53.06, and 49.05 kcal/mol, respectively. The least stabilization energy values for LP1 → σ^* transition are 0.62, 0.54, 0.51, 0.63, 0.53, 0.63, 0.62, and 0.53 kcal/mol observed for LP1(O9) → σ^*(C16−H17), LP2(Cl38) → σ^*(C17−H18), LP2(Cl40) → σ^*(C19−C20), LP1(O9) → σ^*(C16−H17), LP2(Br40) → σ^*(C21−C24), LP1(O40) → σ^*(C21−C24), LP1(O9) → σ^*(C16−H17), and LP1(O9) → σ^*(C16−H17). The aforementioned results therefore showed that the studied compounds had ICT, hyper conjugative interactions, and extended conjugation, which played a significant role in stabilizing these chromophores.

Density of States Analysis. The density of states (DOS) plots are used to support the findings of the FMO analysis by evaluating the behavior of the fragment 1 group in the synthesized compounds (**TCAH1−TCAH8**).[30] Furthermore, these DOS graphs analyze the delocalization of electrons demonstrated in HOMO and LUMO orbitals.[31] Due to the A−π−A architecture of the hydrazone derivatives, the charge distribution of the electronic cloud surrounding the LUMO and HOMO is altered. In Figure 3, the fragment 2 and fragment 1 sections of the compounds used for this investigation are denoted by green and red lines, respectively. The valence band (HOMO) in DOS pictographs exhibits negative values along the *x* axis, while the conduction band (LUMO) displayed positive values. The distance between them served as a visual indicator of the energy gap. By modifying the fragment 2 moieties, the charge distribution is altered, which is further explained by DOS percentages of HOMO and LUMO.

In **TCAH3**, fragment 1 contributes 33.5% to LUMO, while 25% to HOMO. Similarly, fragment 2 contributes 66.5% to LUMO and 74.9% to HOMO. Likewise, in **TCAH1**, **TCAH2**, and **TCAH4−TCAH8** derivatives, fragment 2 manifests the distribution of electronic charges as: 65.9, 56.6, 62.5, 63.0, 59.2, 2.0, and 63.2% to LUMO, whereas 75.4, 81.3, 79.6, 59.1, 76.1, 84.8, and 75.3% to HOMO, respectively. Fragment 1 contributes as: 34.1, 43.4, 37.5, 37.0, 40.8, 98.0, and 38.6% to LUMO and 24.6, 18.7, 20.4, 40.9, 23.9, 15.2, and 24.7% to HOMO, in **TCAH1**, **TCAH2**, and **TCAH4−TCAH8** derivatives, respectively. From Figure 3, it can be seen that the first highest peak of LUMO is exhibited by fragment 1 in all the derivatives at approximately −6 eV; however, in the case of LUMO, the first highest peak is shown by fragment 2 group at approximately −3.5 eV showing a close approximation with FMO diagrams, hence manifesting efficient transfer of charge toward fragment 2. In the examined compounds, there is apparent electron delocalization and a significant quantity of charge is transferred from fragment 1 to fragment 2, according to the overall pattern of charge distribution.

NLO Properties. Conjugated organic molecules have been exploited as advanced materials on a significant scale over the past two decades owing to their intriguingly tremendous NLO response and structural tunability.[32] They have been extensively used in optoelectronics,[33] photonics,[34] data storage,[35] and optical power limiting.[36] To design such materials, one must have a thorough understanding of NLO properties, such as the dipole moment (μ_{tot}), the polarizability (linear), and hyperpolarizability (nonlinear) of the material.[37] The material's electronic characteristics determine the magnitude of the optical response. The estimated values for the linear polarizability $\langle\alpha\rangle$, first hyperpolarizability (β_{tot}), and second hyperpolarizability $\langle\gamma\rangle$, which represent the molecular structure and band gap, are connected to the NLO character. Thus, $\langle\alpha\rangle$, β_{tot}, and $\langle\gamma\rangle$ are computed in order to assess how linear and nonlinear responses are affected by varying fragment 2 moieties in **TCAH1−TCAH8**. The principal findings are provided in Table 4, while other important findings are displayed in Tables S19−S22.

The dipole moment is directly co-related to electronegativity difference as it is observed that more the electronegativity difference larger would be the dipole moment. The data presented in Table S18 revealed that in all the synthesized

https://doi.org/10.1021/acsomega.3c03088
ACS Omega 2023, 8, 27488−27499

Table 4. Computed Average Polarizability $\langle\alpha\rangle$, Dipole Polarizability (μ_{tot}), First (β_{tot}) and Second Hyperpolarizabilities $\langle\gamma\rangle$ of TCAH1−TCAH8

compounds	μ_{total}	$\langle\alpha\rangle \times 10^{-23}$	$\beta_{tot} \times 10^{-29}$	$\langle\gamma\rangle \times 10^{-34}$
TCAH1	3.860	4.591	1.757	1.970
TCAH2	5.946	4.869	1.618	1.806
TCAH3	5.989	4.946	1.668	2.001
TCAH4	3.913	5.157	2.186	2.753
TCAH5	4.632	4.869	1.884	2.074
TCAH6	3.425	5.134	1.667	2.118
TCAH7	3.987	5.136	1.989	2.482
TCAH8	5.105	5.077	1.542	2.337

compounds dipole moment is more prominent along the *x*-axis. The largest magnitude of the μ_{xx} tensor of −1.6972 D is observed in **TCAH8**. μ_{tot} values of **TCAH1−TCAH8** are found to be 3.860, 5.946, 5.989, 3.913, 4.632, 3.425, 3.987, and 5.105 D, respectively. Among all the studied compounds, **TCAH3**, **TCAH2**, and **TCAH8** have showed the highest value of μ_{tot} due to the presence of strong electronegative groups as terminal fragment 2 moieties which effectively pull electrons from fragment 1. On comparison with μ_{tot} of standard *para* nitroaniline (pNA), i.e., 4.9276 D, our computed compounds (**TCAH2**, **TCAH3**, and **TCAH8**) possess 1.207, 1.215, and 1.036 times larger values than pNA, respectively, rendering them highly efficient NLO compounds. The computed dipole moments of the studied chromophores are arranged in the decreasing order as: **TCAH3** > **TCAH2** > **TCAH8** > **TCAH5** > **TCAH7** > **TCAH4** > **TCAH1** > **TCAH6**. It is evident from the data that charge transference increases with increasing μ_{tot} values. Among the synthesized compounds, **TCAH4** has the greatest first-order polarizability value (5.157×10^{-23} esu), while **TCAH1** has the lowest value (4.591×10^{-23} esu). The overall descending order of $\langle\alpha\rangle$ is in the following order: **TCAH4** > **TCAH7** > **TCAH6** > **TCAH8** > **TCAH3** > **TCAH2** = **TCAH5** > **TCAH1**. On correlating energy gap values with linear polarizability of the above-synthesized compounds, it can be seen from Figure 4 that compounds with higher band gap possess less linear polarizability and vice versa. **TCAH3** with the highest band gap of 4.123 eV possesses less linear polarizability of 4.946×10^{-23} esu. On the other hand, **TCAH8** with the lowest band gap possesses a high linear polarizability of 5.077×10^{-23} esu. The intramolecular charge transfer that passes from fragment 1 to fragment 2 moiety is related to the first hyperpolarizability. Comparing $\langle\alpha\rangle$ with standard pNA at 1.240059×10^{-23} esu resulted 3.959, 3.926, 3.989, 4.159, 3.926, 4.140, 4.142, and 4.094 times higher $\langle\alpha\rangle$ values in **TCAH1−TCAH8**, respectively. The stronger the ICT, the greater would be the NLO response, and vice versa.[38]

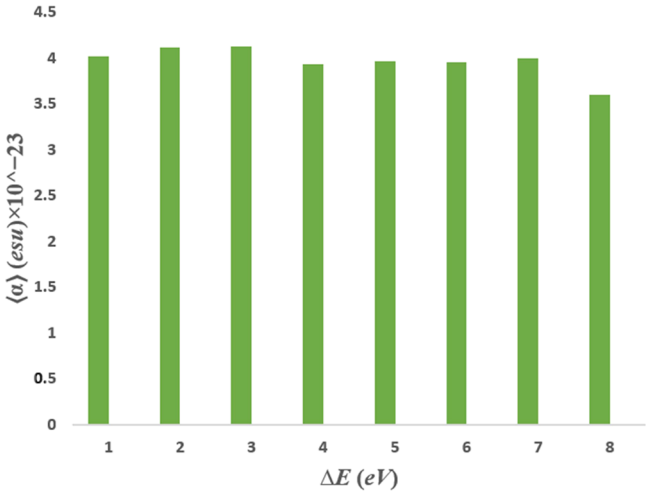

Figure 4. Relation between energy band and linear polarizability values in **TCAH1−TCAH8**.

In the case of second hyperpolarizability, the main contribution to β_{tot} is due to β_{yyy} tensor with a magnitude of 8.575×10^{-31} esu in **TCAH5**, which indicates that a significant amount of charge transfer is observed from fragment 1 to fragment 2 along the *y*-axis. The lowest β_{tot} value among the analyzed compounds is 1.541×10^{-29} esu observed in **TCAH8**, while the greatest β_{tot} value, 2.185×10^{-29} esu, is observed in **TCAH4**. In the synthesized compounds (**TCAH1−TCAH8**), the addition of strongly electron-withdrawing substituents in fragment 2 significantly affects the overall β_{tot} values. The β_{tot} values **TCAH1−TCAH8** are found to be 1.757×10^{-29}, 1.618×10^{-29}, 1.668×10^{-29}, 2.186×10^{-29}, 1.884×10^{-29}, 1.667×10^{-29}, 1.989×10^{-29}, and 1.542×10^{-29} esu. Likewise, the related β_{tot} value of standard pNA (8.123992×10^{-31} esu) with our formulated compounds has resulted in 19.33, 19.92, 20.53, 26.91, 23.19, 20.52, 24.48, and 18.98 times higher values in **TCAH1−TCAH8**, respectively. The descending order of β_{tot} is in good harmony with the descending order of $\langle\alpha\rangle$, which in turn directly opposes the reverse order of E_{gap}. This order demonstrates that **TCAH4** is the most suitable developed structure, which exhibits an efficient NLO response. In addition, compound **TCAH4** has the highest second hyperpolarizability $\langle\gamma\rangle$ value of 2.753×10^{-34} esu, whereas the compound **TCAH2** exhibits the lowest $\langle\gamma\rangle$ value of 1.806×10^{-34} esu. The decreasing order of $\langle\gamma\rangle$ values of synthesized compounds is in the following order: **TCAH4** > **TCAH7** > **TCAH8** > **TCAH6** > **TCAH5** > **TCAH3** > **TCAH1** > **TCAH2**. The $\langle\gamma\rangle$ value of standard pNA corresponds to 4.193974×10^{-36} esu, which is lower than the values of our formulated compounds. Concluding the above analysis, it is determined that the **TCAH4** compound exhibits the highest nonlinearity among the studied derivatives and can be applicable in future high-tech devices. From the literature study, it was observed that E_{gap} influences a molecule's polarizability. A small energy gap is required to express significant linear polarizability.

Natural Population Analysis (NPA). The charge distribution on an atom significantly affects the dipole moment, chemical reactivity, electrostatic interactions between atoms and molecules, as well as several other aspects of the chemical system.[39,40] Moreover, the atomic charge transformation process that takes place in reactions and electrostatic potential on external surfaces of systems may be characterized by Mulliken population analysis.[41] The molecular shape and bonding capacity are significantly influenced by the electrical charges of atoms.[42] The Mulliken population statistics revealed that when additional electronegative elements like O- and N- are added, the electron density across the benzene rings redistributes unevenly.[43] Our focus is on providing the most detailed description of the electron distribution over the synthesized compounds and on evaluating the reactivity of the calculated charges using a quantum chemical perspective.[44] Additionally, a Mulliken population analysis has shown that all of the hydrogen atoms have the same charge distribution. Here, it is evident that C-atom as C1 showed a higher negative

https://doi.org/10.1021/acsomega.3c03088
ACS Omega 2023, 8, 27488−27499

charge (0.38 *e*) and C9 has shown a higher positive charge (0.5 *e*) in **TCAH3** and **TCAH2**. In **TCAH5**, a higher negative charge was shown by C1 (0.38 *e*) and a higher positive charge was shown by C8 (0.5 *e*). In **TCAH 1**, **TCAH7**, and **TCAH4**, a higher negative charge was displayed by O9 (0.39 *e*), and a higher positive charge was revealed by C8 (0.5 *e*), in **TCAH8**, a higher negative charge was shown by N6 (0.38 *e*), while a higher positive charge exhibited by C8 (0.5 *e*). In **TCAH7**, a higher negative charge is shown by O6 (0.39 *e*) and a higher positive charge is shown by C8 (0.5 *e*). In **TCAH7**, all carbon atoms were negatively charged except C2, C3, C8, C14, and C16 due to their attachment to a nitrogen atom. The Mulliken charge distribution of **TCAH1**−**TCAH8** is displayed in Figure S4.

CONCLUSIONS

In the current study, thiazole-based hydrazones (**TCAH1**−**TCAH8**) with the A−π−A framework were synthesized through a condensation reaction. Structural confirmation is accomplished through spectroscopic techniques (^{1}H-, ^{13}C-NMR, and HRMS). Various analyses such as absorption spectra, NLO characteristics, DOS and molecular orbital energies, etc., of synthesized compounds were investigated through DFT. FMO findings elucidate that E_{gap} in **TCAH8** (3.595 eV) was observed to be smaller than those in **TCAH1**−**TCAH7** (3.932−4.123 eV). Moreover, the FMO analysis demonstrated that fragment 1 among derivatives effectively facilitates the transfer of charge between fragment 2 moieties, and the results are also supported by DOS graphs. The NBO study also explored noncovalent interactions, which have been shown to significantly increase the stability of the compound. In **TCAH8**, the maximum red-shifted absorption was found at 342.9 nm, with the lowest transition energy (3.615 eV) and the greatest oscillation intensity (0.785). Interestingly the $\langle\alpha\rangle$, (β_{tot}), and $\langle\gamma\rangle$ values for **TCAH4** were found to be 5.157 × 10^{-23}, 2.185 × 10^{-29}, and 2.753 × 10^{-34} esu, respectively, which are larger than others, rendering **TCAH4** with highest NLO behavior. These significant NLO results of designed chromophores revealed that these materials might be utilized as efficient optoelectronic materials.

EXPERIMENTAL SECTION

General Method for the Synthesis of *N*′-Arylidene-2-(2-arylidenehydrazinyl)thiazole-4-carbohydrazides (TCAH1−TCAH8). The desired *N*′-arylidene-2-(2-arylidenehydrazinyl)thiazole-4-carbohydrazides (**TCAH1**−**TCAH8**) were synthesized by mixing 2-(2-(arylidene)-hydrazinyl)thiazole-4-carbohydrazides (1.0 mmol) with aryl aldehydes (1.0 mmol) under reflux for 8−12 h in methanol solvent, using acetic acid as catalyst. The progress of the reaction mixture was observed with TLC after every 30 min. The appearance of a single spot at TLC indicated the completion of the reaction. The hot reaction mixture was left to attain the room temperature. The reaction mixture was then put on crushed ice. The appearance of precipitates was observed. The obtained solid was filtered under vacuum and washed with plenty of cold water to remove the mother liquor from the collected solid. TLC pure compounds were characterized with proton and carbon NMR and HRMS spectroscopic techniques.

***N*′-Benzylidene-2-(2-benzylidenehydrazinyl)thiazole-4-carbohydrazide (TCAH1).** Light green solid; yield: 76%; melting point: 286−288 °C; R_f: 0.51 (acetone/*n*-hexane, 1:3); ^{1}H-NMR (500 MHz): δ 7.43 (6H, m, Ar−H), 7.69 (5H, m, Ar−H), 8.10 (1H, s, 1,3-thiazole ring C-5), 8.47 (1H, s, −CH═N− azomethine), 11.33 (1H, s, −NH−N═), 12.05 (1H, s, −NH−CO−); ^{13}C-NMR (126 MHz): δ 115.6 (1,3-thiazole ring C-5), 126.8, 127.6, 129.3, 129.3, 130.5, 134.6, 134.8 (Ar−C), 142.8 (−CH═N− azomethine), 145.7 (−CH═N− azomethine), 148.5 (1,3-thiazole ring C-4), 157.8 (−CO−NH−), 168.9 (1,3-thiazole ring C-2); HRMS: *m*/*z* for $C_{18}H_{15}N_5OS$, calcd (M + H^+): 350.1076, found; 350.1063, calcd (M + Na^+): 372.0895, found; 372.0875, calcd (2 M + Na^+): 721.1892, found; 721.1864.

***N*′-(2-Chlorobenzylidene)-2-(2-(2-chlorobenzylidene)hydrazinyl)thiazole-4-carbohydrazide (TCAH2).** Off-white solid; yield: 73%; melting point: 230−232 °C; R_f: 0.47 (acetone/*n*-hexane, 1:3); ^{1}H-NMR (500 MHz): δ 7.42 (4H, m, Ar−H), 7.50 (2H, m, Ar−H), 7.92 (1H, dd, Ar−H, *J* = 2.41, 7.14 Hz), 8.00 (1H, dd, Ar−H, *J* = 2.56, 6.75 Hz), 7.75 (1H, s, 1,3-thiazole ring C-5), 8.47 (1H, s, −CH═N− azomethine), 8.91 (1H, s, −CH═N− azomethine), 11.77 (1H, s, −NH−N═), 12.27 (1H, s, −NH−CO−); ^{13}C-NMR (126 MHz): δ 109.9 (1,3-thiazole ring C-5), 116.4, 126.7, 127.4, 128.0, 128.1, 130.4, 131.3, 131.8, 131.9, 132.2, 132.8, 133.7 (Ar−C), 138.6 (−CH═N− azomethine), 144.5 (−CH═N− azomethine), 145.7 (1,3-thiazole ring C-4), 157.9 (−CO−NH−), 168.5 (1,3-thiazole ring C-2); HRMS: *m*/*z*. For $C_{18}H_{13}Cl_2N_5OS$, calcd (M + H^+): 418.028, found; 418.0286, calcd (2M + Na^+): 857.02, found; 857.0295.

***N*′-(3-Chlorobenzylidene)-2-(2-(3-chlorobenzylidene)hydrazinyl)thiazole-4-carbohydrazide (TCAH3).** Off-white solid; yield: 98%; melting point: 238−240 °C; R_f: 0.44 (acetone/*n*-hexane, 1:3); ^{1}H-NMR (500 MHz): δ 7.46 (4H, m, Ar−H), 7.62 (2H, m, Ar−H), 7.73 (2H, d, Ar−H, *J* = 4.90 Hz), 7.69 (1H, s, 1,3-thiazole ring C-5), 8.08 (1H, s, −CH═N− azomethine), 8.45 (1H, s, −CH═N− azomethine), 11.47 (1H, s, −NH−N═), 12.22 (1H, s, −NH−CO−); ^{13}C-NMR (126 MHz): δ 116.2 (1,3-thiazole ring C-5), 125.5, 126.1, 126.3, 126.7, 129.5, 130.1, 131.2, 134.1 (Ar−C), 136.9 (−CH═N− azomethine), 137.0 (−CH═N− azomethine), 146.8 (1,3-thiazole ring C-4), 157.9 (−CO−NH−), 168.6 (1,3-thiazole ring C-2); HRMS: *m*/*z*. For $C_{18}H_{13}Cl_2N_5OS$, calcd (2M + Na^+): 857.02, found; 857.0301.

***N*′-(4-Chlorobenzylidene)-2-(2-(4-chlorobenzylidene)hydrazinyl)thiazole-4-carbohydrazide (TCAH4).** Off-white solid; yield: 77%; melting point: 289−291 °C; R_f: 0.44 (acetone/*n*-hexane, 1:3); ^{1}H-NMR (500 MHz): δ 7.51 (4H, m, Ar−H), 7.70 (5H, m, Ar−H), 8.09 (1H, s, 1,3-thiazole ring C-5), 8.46 (1H, s, −CH═N− azomethine), 11.40 (1H, s, −NH−N═), 12.15 (1H, s, −NH−CO−); ^{13}C-NMR (126 MHz): δ 115.9 (1,3-thiazole ring C-5), 126.1, 128.4, 129.2, 129.4, 131.2, 133.7, 134.3, 134.9 (Ar−C), 136.9 (−CH═N− azomethine), 141.5 (−CH═N− azomethine), 147.2 (1,3-thiazole ring C-4), 157.8 (−CO−NH−), 168.6 (1,3-thiazole ring C-2); HRMS: *m*/*z*. For $C_{18}H_{13}Cl_2N_5OS$, calcd (2M + Na^+): 857.02, found; 857.0314.

***N*′-(2-Bromobenzylidene)-2-(2-(2-bromobenzylidene)hydrazinyl)thiazole-4-carbohydrazide (TCAH5).** Off-white solid; yield: 75%; melting point: 231−233 °C; R_f: 0.42 (acetone/*n*-hexane, 1:3); ^{1}H-NMR (500 MHz): δ 7.34 (2H, m, Ar−H), 7.45 (2H, t, Ar−H, *J* = 7.55 Hz), 7.67 (2H, m, Ar−H), 7.75 (1H, s, 1,3-thiazole ring C-5), 7.91 (1H, dd, Ar−H, *J* = 1.79, 7.94 Hz), 7.98 (1H, dd, Ar−H, *J* = 1.80, 7.90 Hz), 8.44 (1H, s, −CH═N− azomethine), 8.86

https://doi.org/10.1021/acsomega.3c03088
ACS Omega 2023, 8, 27488−27499

(1H, s, −CH═N− azomethine), 11.81 (1H, s, −NH−N═), 12.31 (1H, s, −NH−CO−); ^{13}C-NMR (126 MHz): δ 116.4 (1,3-thiazole ring C-5), 123.2, 124.0, 127.1, 127.8, 128.5, 128.6, 131.6, 132.1, 132.4, 133.3, 133.6, 133.7 (Ar−C), 140.8 (−CH═N− azomethine), 145.8 (−CH═N− azomethine), 146.9 (1,3-thiazole ring C-4), 157.9 (−CO−NH−), 168.5 (1,3-thiazole ring C-2); HRMS: *m*/*z*. For $C_{18}H_{13}Br_2N_5OS$, calcd (M + H$^+$): 505.928, found; 505.9267.

***N′*-(2-Methylbenzylidene)-2-(2-(2-methylbenzylidene)hydrazinyl)thiazole-4-carbohydrazide (TCAH6).** Off-white solid; yield: 81%; melting point: 241−243 °C; R_f: 0.31 (acetone/*n*-hexane, 1:3); ^{1}H-NMR (300 MHz): δ 2.47 (6H, m, 2-CH$_3$), 7.28 (6H, m, Ar−H), 7.71 (2H, m, Ar−H), 7.84 (1H, s, 1,3-thiazole ring C-5), 8.37 (1H, s, −CH═N− azomethine), 8.80 (1H, s, −CH═N− azomethine), 11.38 (1H, s, −NH−N═), 12.01 (1H, s, −NH−CO−); ^{13}C-NMR (75 MHz): δ 19.5 (−CH$_3$), 20.2 (−CH$_3$), 115.6 (1,3-thiazole ring C-5), 126.3, 126.6, 126.7, 126.8, 129.7, 130.2, 131.3, 131.5, 132.5, 132.8, 136.6, 137.5, (Ar−C), 142.2 (−CH═N− azomethine), 147.3 (1,3-thiazole ring C-4), 157.7 (−CO−NH−), 168.9 (1,3-thiazole ring C-2); HRMS: *m*/*z*. For $C_{20}H_{19}N_5OS$, calcd (M + H$^+$): 378.138, found; 378.1377, calcd (M + Na$^+$) 400.11, found; 400.1195; calcd (2 M + Na$^+$): 777.24, found; 777.2495.

***N′*-(4-Methylbenzylidene)-2-(2-(4-methylbenzylidene)hydrazinyl)thiazole-4-carbohydrazide (TCAH7).** White solid; yield: 65%; melting point: 293−295 °C; R_f: 0.35 (acetone/*n*-hexane, 1:3); ^{1}H-NMR (500 MHz): δ 2.32 (6H, d, 2-CH$_3$, *J* = 5.00 Hz), 7.25 (4H, m, Ar−H), 7.55 (2H, d, Ar−H, *J* = 6.63 Hz), 7.59 (2H, d, Ar−H, *J* = 6.97 Hz), 7.66 (1H, s, 1,3-thiazole ring C-5), 8.07 (1H, s, −CH═N− azomethine), 8.42 (1H, s, −CH═N− azomethine), 11.24 (1H, s, −NH−N═), 11.97 (1H, s, −NH−CO−); ^{13}C-NMR (126 MHz): δ 21.5, 21.5 (2-CH$_3$), 115.4 (1,3-thiazole ring C-5), 126.8, 127.6, 129.8, 129.9, 131.9, 132.1, 139.7, 142.9 (Ar−C), 140.3 (−CH═N− azomethine), 145.8 (−CH═N− azomethine), 148.5 (1,3-thiazole ring C-4), 157.7 (−CO−NH−), 168.8 (1,3-thiazole ring C-2); HRMS: *m*/*z*. For $C_{20}H_{19}N_5OS$, calcd (M + H$^+$): 378.138, found; 378.1377, calcd (M + Na$^+$) 400.11, found; 400.1197; calcd (2M + Na$^+$): 777.24, found; 777.2492.

***N′*-(2-Nitrobenzylidene)-2-(2-(3-nitrobenzylidene)-hydrazinyl)thiazole-4-carbohydrazide (TCAH8).** Dark yellow solid; yield: 80%; melting point: 241−242 °C; R_f: 0.36 (acetone/*n*-hexane, 1:3); ^{1}H-NMR (300 MHz): δ 7.51 (1H, s, 1,3-thiazole ring C-5), 7.75 (3H, m, Ar−H), 8.09 (2H, t, Ar−H, *J* = 8.10 Hz), 8.20 (2H, t, Ar−H, *J* = 7.20 Hz), 8.46 (2H, d, Ar−H, *J* = 8.10 Hz), 8.90 (1H, s, −CH═N− azomethine), 9.07 (1H, s, −CH═N− azomethine), 11.86 (1H, s, −NH−N═), 12.44 (1H, s, −NH−CO−); ^{13}C-NMR (75 MHz): δ 116.7 (1,3-thiazole ring C-5), 119.9, 120.8, 123.9, 125.1, 128.5, 129.2, 130.9, 131.2, 132.8, 132.9, 134.2, 136.5 (Ar−C), 136.6 (−CH═N− azomethine), 139.9 (−CH═N− azomethine), 140.4 (1,3-thiazole ring C-4), 148.7 (−CO−NH−), 168.3 (1,3-thiazole ring C-2); HRMS: *m*/*z*. For $C_{20}H_{19}N_5OS$, calcd (M + Na$^+$) 462.05, found; 462.0583.

COMPUTATIONAL PROCEDURE

To probe the NLO properties of the synthesized compounds, Gaussian 16 program[45] was utilized. At first, the structures of **TCAH1−TCAH8** were optimized at B3PW91/6-311G(d,p) level of DFT/TDDFT,[14] and the absence of any negative vibrational frequency indicated the successful optimization of geometries. For the preparation of input structures and visualization of the optimized geometries, GaussView 6.0[46] program was utilized. The time-dependent DFT (TD-B3PW91) was utilized to investigate UV−vis spectrum and frontier molecular orbital (FMO) investigations. With the aid of Avogadro software,[47] the HOMO and LUMO orbitals and energies of molecules were drawn. The DOS pictographs were plotted using the PyMOlyze program.[48] By using the energies of HOMOs and LUMOs of prepared compounds, their global reactivity descriptors were also interpreted using Koopman's theorem.[49,50]

$$E_g = E_{LUMO} - E_{HOMO} \quad (1)$$

$$\mu = \frac{(E_{LUMO} + E_{HOMO})}{2} \quad (2)$$

$$\eta = IP - EA \quad (3)$$

$$\sigma = \frac{1}{\eta} \quad (4)$$

$$\omega = \frac{\mu^2}{2\eta} \quad (5)$$

$$\Delta N_{max} = \frac{-\mu}{\eta} \quad (6)$$

NBO 3.1 program[51] was utilized to calculated NBO study. Furthermore, the total static dipole moment (μ_{tot}),[52] polarizability $\langle\alpha\rangle$,[53] and nonlinear polarizabilities (β_{tot}[54] and $\langle\gamma\rangle$[55]) were calculated via the following chemical equations:

$$\mu = (\mu^2_x + \mu^2_y + \mu^2_z)^{1/2} \quad (7)$$

$$\langle\alpha\rangle = 1/3(\alpha_{xx} + \alpha_{yy} + \alpha_{zz}) \quad (8)$$

$$\beta_{tot} = (\beta_x^2 + \beta_y^2 + \beta_z^2)^{1/2} \quad (9)$$

$$\gamma_{tot} = \sqrt{\gamma_x^2 + \gamma_y^2 + \gamma_z^2} \quad (10)$$

ASSOCIATED CONTENT

Supporting Information

The Supporting Information is available free of charge at https://pubs.acs.org/doi/10.1021/acsomega.3c03088.

UV−Vis data (wavelength, excitation energies and oscillator strengths), FMO, NPA, and NLO of reported chromophores calculated using the B3PW91/6-311G-(d,p) method and spectra of ^{1}H-, ^{13}C-NMR, and HRMS (PDF)

AUTHOR INFORMATION

Corresponding Authors

Tashfeen Akhtar − *Department of Chemistry, Mirpur University of Science and Technology (MUST), 10250 Mirpur, AJ&K, Pakistan*; Email: tashfeenchem@must.edu.pk

Muhammad Khalid − *Institute of Chemistry and Centre for Theoretical and Computational Research, Khwaja Fareed University of Engineering & Information Technology, Rahim Yar Khan 64200, Pakistan*; orcid.org/0000-0002-1899-5689; Email: khalid@iq.usp.br

https://doi.org/10.1021/acsomega.3c03088
ACS Omega 2023, 8, 27488−27499

Suvash Chandra Ojha − *Department of Infectious Diseases, The Affiliated Hospital of Southwest Medical University, Luzhou 646000, China*; Email: suvash_ojha@swmu.edu.cn

Authors

Muhammad Haroon − *Department of Chemistry, Mirpur University of Science and Technology (MUST), 10250 Mirpur, AJ&K, Pakistan; Department of Chemistry and Biochemistry, Miami University, Oxford, Ohio 45056, United States*

Qurat-ul-ain Shaikh − *Institute of Chemistry, Shah Abdul Latif University, Khairpur 66111, Pakistan*

Hasnain Mehmood − *Department of Chemistry, Mirpur University of Science and Technology (MUST), 10250 Mirpur, AJ&K, Pakistan*

Muhammad Adnan Asghar − *Department of Chemistry, Division of Science and Technology, University of Education, Lahore 89002, Pakistan*

Saad M. Alshehri − *Department of Chemistry, College of Science, King Saud University, Riyadh 11451, Saudi Arabia*

Complete contact information is available at: https://pubs.acs.org/10.1021/acsomega.3c03088

Notes

The authors declare no competing financial interest.

■ ACKNOWLEDGMENTS

M.K. gratefully acknowledges the financial support of HEC Pakistan (project no. 20-14703/NRPU/R&D/HEC/2021). The authors are also thankful for cooperation and collaboration of A.A.C.B. from IQ-USP, Brazil, especially for his continuous support and providing computational lab facilities. The authors thank the Researchers Supporting Project number (RSP2023R29), King Saud University, Riyadh, Saudi Arabia. S.C.O. acknowledges the support from the doctoral research fund of the Affiliated Hospital of Southwest Medical University.

■ REFERENCES

(1) Khaliq, F.; Ayub, K.; Mahmood, T.; Muhammad, S.; Tabassum, S.; Gilani, M. A. First Example of Lanthanum as Dopant on Al12N12 and Al12P12 Nanocages for Improved Electronic and Nonlinear Optical Properties with High Stability. *Mater. Sci. Semicond. Process.* **2021**, *135*, No. 106122.

(2) Mahmood, A.; Sandali, Y.; Wang, J.-L. Easy and Fast Prediction of Green Solvents for Small Molecule Donor-Based Organic Solar Cells through Machine Learning. *Phys. Chem. Chem. Phys.* **2023**, *25*, 10417−10426.

(3) Vijayalakshmi, S.; Kalyanaraman, S. DFT and TD-DFT Approach for the Analysis of NLO and OLED Applications of 9-Anthraldehyde. *Optik* **2014**, *125*, 2429−2432.

(4) Andraud, C.; Brotin, T.; Garcia, C.; Pelle, F.; Goldner, P.; Bigot, B.; Collet, A. Theoretical and Experimental Investigations of the Nonlinear Optical Properties of Vanillin, Polyenovanillin, and Bisvanillin Derivatives. *J. Am. Chem. Soc.* **1994**, *116*, 2094−2102.

(5) Liyanage, P. S.; de Silva, R. M.; de Silva, K. M. N. Nonlinear Optical (NLO) Properties of Novel Organometallic Complexes: High Accuracy Density Functional Theory (DFT) Calculations. *THEOCHEM* **2003**, *639*, 195−201.

(6) Hohenberg, P.; Kohn, W. Inhomogeneous Electron Gas. *Phys. Rev.* **1964**, *136*, B864−B871.

(7) Islam, N.; Chimni, S. S. DFT Investigation on Nonlinear Optical (NLO) Properties of Novel Borazine Derivatives. *Comput. Theor. Chem.* **2016**, *1086*, 58−66.

(8) Pan, F.; Wong, M. S.; Bösch, M.; Bosshard, C.; Meier, U.; Günter, P. A Highly Efficient Organic Second-Order Nonlinear Optical Crystal Based on a Donor-Acceptor Substituted 4-Nitrophenylhydrazone. *Appl. Phys. Lett.* **1997**, *71*, 2064−2066.

(9) Zhang, C.; Li, X.; Wang, Y.; An, M.; Sun, Z. A Hydrazone Organic Optical Modulator with a π Electronic System for Ultrafast Photonics. *J. Mater. Chem. C* **2021**, *9*, 11306−11313.

(10) Xu, W.; Shao, Z.; Han, Y.; Wang, W.; Song, Y.; Hou, H. Light-Adjustable Third-Order Nonlinear Absorption Properties Based on a Series of Hydrazone Compounds. *Dyes Pigm.* **2018**, *152*, 171−179.

(11) Achelle, S.; Baudequin, C.; Plé, N. Luminescent Materials Incorporating Pyrazine or Quinoxaline Moieties. *Dyes Pigm.* **2013**, *98*, 575−600.

(12) Niehaus, T. A.; Suhai, S.; Della Sala, F.; Lugli, P.; Elstner, M.; Seifert, G.; Frauenheim, T. Tight-Binding Approach to Time-Dependent Density-Functional Response Theory. *Phys. Rev. B* **2001**, *63*, No. 085108.

(13) Lu, J.; Zhang, L.; Liu, L.; Liu, G.; Jia, D.; Wu, D.; Xu, G. Study of Fluorescence Properties of Several 4-Acyl Pyrazolone Derivatives and Their Zn (II) Complexes. *Spectrochim. Acta, Part A* **2008**, *71*, 1036−1041.

(14) Khalid, M.; Khan, M. U.; Shafiq, I.; Hussain, R.; Mahmood, K.; Hussain, A.; Jawaria, R.; Hussain, A.; Imran, M.; Assiri, M. A.; Ali, A.; ur Rehman, M. F.; Sun, K.; Li, Y. NLO Potential Exploration for D−π−A Heterocyclic Organic Compounds by Incorporation of Various π-Linkers and Acceptor Units. *Arab. J. Chem.* **2021**, *14*, No. 103295.

(15) Khalid, M.; Lodhi, H. M.; Khan, M. U.; Imran, M. Structural Parameter-Modulated Nonlinear Optical Amplitude of Acceptor−π−D−π−Donor-Configured Pyrene Derivatives: A DFT Approach. *RSC Adv.* **2021**, *11*, 14237−14250.

(16) Khalid, M.; Ali, A.; Jawaria, R.; Asghar, M. A.; Asim, S.; Khan, M. U.; Hussain, R.; Fayyaz ur Rehman, M.; Ennis, C. J.; Akram, M. S. First Principles Study of Electronic and Nonlinear Optical Properties of A−D−π−A and D−A−D−π−A Configured Compounds Containing Novel Quinoline−Carbazole Derivatives. *RSC Adv.* **2020**, *10*, 22273−22283.

(17) Khan, B.; Khalid, M.; Shah, M. R.; Tahir, M. N.; Asif, H. M.; Rahnamaye Aliabad, H. A.; Hussain, A. Synthetic, Spectroscopic, SC-XRD and Nonlinear Optical Analysis of Potent Hydrazide Derivatives: A Comparative Experimental and DFT/TD-DFT Exploration. *J. Mol. Struct.* **2020**, *1200*, No. 127140.

(18) Pearson, R. G. Absolute Electronegativity and Absolute Hardness of Lewis Acids and Bases. *J. Am. Chem. Soc.* **1985**, *107*, 6801−6806.

(19) Parr, R. G.; Yang, W. Density Functional Approach to the Frontier-Electron Theory of Chemical Reactivity. *J. Am. Chem. Soc.* **1984**, *106*, 4049−4050.

(20) Parr, R. G.; Donnelly, R. A.; Levy, M.; Palke, W. E. Electronegativity: The Density Functional Viewpoint. *J. Chem. Phys.* **1978**, *68*, 3801−3807.

(21) Parthasarathi, R.; Padmanabhan, J.; Elango, M.; Subramanian, V.; Chattaraj, P. K. Intermolecular Reactivity through the Generalized Philicity Concept. *Chem. Phys. Lett.* **2004**, *394*, 225−230.

(22) Parr, R. G.; Pearson, R. G. Absolute Hardness: Companion Parameter to Absolute Electronegativity. *J. Am. Chem. Soc.* **1983**, *105*, 7512−7516.

(23) Politzer, P.; Truhlar, D. G. Introduction: The Role of the Electrostatic Potential in Chemistry. In *Chemical Applications of Atomic and Molecular Electrostatic Potentials: Reactivity, Structure, Scattering, and Energetics of Organic, Inorganic, and Biological Systems*; 1981, pp 1−6.

(24) Chattaraj, P. K.; Roy, D. R. Update 1 of: Electrophilicity Index. *Chem. Rev.* **2007**, *107*, PR46−PR74.

(25) Oudar, J.-L.; Chemla, D. S. Hyperpolarizabilities of the Nitroanilines and Their Relations to the Excited State Dipole Moment. *J. Chem. Phys.* **1977**, *66*, 2664−2668.

(26) Tahir, M. N.; Khalid, M.; Islam, A.; Mashhadi, S. M. A.; Braga, A. A. Facile Synthesis, Single Crystal Analysis, and Computational

Studies of Sulfanilamide Derivatives. *J. Mol. Struct.* **2017**, *1127*, 766−776.
(27) Mahmood, A.; Khan, S. U.-D.; Rana, U. A.; Tahir, M. H. Red Shifting of Absorption Maxima of Phenothiazine Based Dyes by Incorporating Electron-Deficient Thiadiazole Derivatives as π-Spacer. *Arab. J. Chem.* **2019**, *12*, 1447−1453.
(28) Politzer, P.; Truhlar, D. G. *Chemical Applications of Atomic and Molecular Electrostatic Potentials: Reactivity, Structure, Scattering, and Energetics of Organic, Inorganic, and Biological Systems*; Springer Science & Business Media, 2013.
(29) Kaur, M.; Sheena Mary, Y.; Varghese, H. T.; Yohannan Panicker, C.; Yathirajan, H. S.; Siddegowda, M. S.; Alsenoy, C. V. Vibrational Spectroscopic, Molecular Structure, First Hyperpolarizability and NBO Studies of 4′-Methylbiphenyl-2-Carbonitrile. *Spectrochim. Acta, Part A* **2012**, *98*, 91−99.
(30) Khalid, M.; Shafiq, I.; Zhu, M.; Khan, M. U.; Shafiq, Z.; Iqbal, J.; Alam, M. M.; Braga, A. A. C.; Imran, M. Efficient Tuning of Small Acceptor Chromophores with A1-π-A2-π-A1 Configuration for High Efficacy of Organic Solar Cells via End Group Manipulation. *J. Saudi Chem. Soc.* **2021**, *25*, No. 101305.
(31) Ans, M.; Iqbal, J.; Ahmad, Z.; Muhammad, S.; Hussain, R.; Eliasson, B.; Ayub, K. Designing Three-Dimensional (3D) Non-Fullerene Small Molecule Acceptors with Efficient Photovoltaic Parameters. *ChemistrySelect* **2018**, *3*, 12797−12804.
(32) Recatalá, D.; Llusar, R.; Barlow, A.; Wang, G.; Samoc, M.; Humphrey, M. G.; Guschin, A. L. Synthesis and Optical Power Limiting Properties of Heteroleptic Mo 3 S 7 Clusters. *Dalton Trans.* **2015**, *44*, 13163−13172.
(33) Schmitt, J.; Heitz, V.; Sour, A.; Bolze, F.; Ftouni, H.; Nicoud, J.-F.; Flamigni, L.; Ventura, B. Diketopyrrolopyrrole-Porphyrin Conjugates with High Two-Photon Absorption and Singlet Oxygen Generation for Two-Photon Photodynamic Therapy. *Angew. Chem., Int. Ed.* **2015**, *54*, 169−173.
(34) Braga, A. A.; Morgon, N. H.; Ujaque, G.; Maseras, F. Computational Characterization of the Role of the Base in the Suzuki-Miyaura Cross-Coupling Reaction. *J. Am. Chem. Soc.* **2005**, *127*, 9298−9307.
(35) Zhang, Y.; Xie, S.; Zeng, Z.; Tang, B. Z. Functional Scaffolds from AIE Building Blocks. *Matter* **2020**, *3*, 1862−1892.
(36) Durand, R. J.; Achelle, S.; Gauthier, S.; Cabon, N.; Ducamp, M.; Kahlal, S.; Saillard, J.-Y.; Barsella, A.; Robin-Le Guen, F. Incorporation of a Ferrocene Unit in the π-Conjugated Structure of Donor-Linker-Acceptor (D-π-A) Chromophores for Nonlinear Optics (NLO). *Dyes Pigm.* **2018**, *155*, 68−74.
(37) Khan, I.; Khalid, M.; Adeel, M.; Niaz, S. I.; Shafiq, I.; Muhammad, S.; Braga, A. A. C. Palladium-Catalyzed Synthesis of 5-(Arylated) Pyrimidines, Their Characterization, Electronic Communication, and Non-Linear Optical Evaluations. *J. Mol. Struct.* **2021**, *1237*, No. 130408.
(38) Qin, C.; Clark, A. E. DFT Characterization of the Optical and Redox Properties of Natural Pigments Relevant to Dye-Sensitized Solar Cells. *Chem. Phys. Lett.* **2007**, *438*, 26−30.
(39) Khalid, M.; Khan, M.; Shafiq, I.; Mahmood, K.; Nadeem Akhtar, M.; Iqbal, J.; Al-Sadoon, M. K.; Zaman, W.; Carmo Braga, A. A. Role of Donors in Triggering Second Order Non-Linear Optical Properties of Non-Fullerene FCO-2FR1 Based Derivatives: A Theoretical Perspective. *Heliyon* **2023**, *9*, No. e13033.
(40) Bullo, S.; Jawaria, R.; Faiz, I.; Shafiq, I.; Khalid, M.; Asghar, M. A.; Baby, R.; Orfali, R.; Perveen, S. Efficient Synthesis, Spectroscopic Characterization, and Nonlinear Optical Properties of Novel Salicylaldehyde-Based Thiosemicarbazones: Experimental and Theoretical Studies. *ACS Omega* **2023**, 13982.
(41) Mulliken, R. S. Electronic Population Analysis on LCAO−MO Molecular Wave Functions. I. *J. Chem. Phys.* **1955**, *23*, 1833−1840.
(42) Khalid, M.; Nadeem Arshad, M.; Murtaza, S.; Shafiq, I.; Haroon, M.; Asiri, A. M.; AlcântaraMorais, S. F. d.; Braga, A. A. C. Enriching NLO Efficacy via Designing Non-Fullerene Molecules with the Modification of Acceptor Moieties into ICIF2F: An Emerging Theoretical Approach. *RSC Adv.* **2022**, *12*, 13412−13427.
(43) Li, L.; Wu, C.; Wang, Z.; Zhao, L.; Li, Z.; Sun, C.; Sun, T. Density Functional Theory (DFT) and Natural Bond Orbital (NBO) Study of Vibrational Spectra and Intramolecular Hydrogen Bond Interaction of l-Ornithine−l-Aspartate. *Spectrochim. Acta, Part A* **2015**, *136*, 338−346.
(44) Burrows, J. A. Pauling, Linus. The Nature of the Chemical Bond and the Structure of Molecules Aid Crystals. Ithaca: The Cornell University Press, 1939. 430 p. $4.50. *Sci. Educ.* **1941**, *25*, 120.
(45) Frisch, M.; Trucks, G. W.; Schlegel, H. B.; Scuseria, G. E.; Robb, M. A.; Cheeseman, J. R.; Scalmani, G.; Barone, V.; Petersson, G. A.; Nakatsuji, H. *Gaussian 16*; 2016.
(46) Dennington, R.; Keith, T. A.; Millam, J. M. *GaussView 6.0. 16*; Semichem Inc.: Shawnee Mission, KS 2016.
(47) Hanwell, M. D.; Curtis, D. E.; Lonie, D. C.; Vandermeersch, T.; Zurek, E.; Hutchison, G. R. Avogadro: An Advanced Semantic Chemical Editor, Visualization, and Analysis Platform. *J. Cheminf.* **2012**, *4*, 17.
(48) Tenderholt, A. L. *PyMOlyze, Version 2.0*; 2007.
(49) Mirkamali, E. S.; Ahmadi, R.; Kalateh, K.; Zarei, G. Adsorption of Melphalan Anticancer Drug on the Surface of Fullerene (C 24): A Comprehensive DFT Study. *Nanomed. J.* **2019**, *6*, 112−119.
(50) Koopmans, T. Über Die Zuordnung von Wellenfunktionen Und Eigenwerten Zu Den Einzelnen Elektronen Eines Atoms. *Physica* **1934**, *1*, 104−113.
(51) Glendening, E. D.; Landis, C. R.; Weinhold, F. Natural Bond Orbital Methods. *Wiley Interdiscip. Rev.: Comput. Mol. Sci.* **2012**, *2*, 1−42.
(52) Hudson, J. J.; Sauer, B. E.; Tarbutt, M. R.; Hinds, E. A. Measurement of the Electron Electric Dipole Moment Using YbF Molecules. *Phys. Rev. Lett.* **2002**, *89*, No. 023003.
(53) Alparone, A. Linear and Nonlinear Optical Properties of Nucleic Acid Bases. *Chem. Phys.* **2013**, *410*, 90−98.
(54) Plaquet, A.; Guillaume, M.; Champagne, B.; Castet, F.; Ducasse, L.; Pozzo, J.-L.; Rodriguez, V. In Silico Optimization of Merocyanine-Spiropyran Compounds as Second-Order Nonlinear Optical Molecular Switches. *Phys. Chem. Chem. Phys.* **2008**, *10*, 6223−6232.
(55) Boyd, D. B.; Lipkowitz, K. B. *Reviews in Computational Chemistry, Volume 5*; John Wiley & Sons, 2009; vol 5.

https://doi.org/10.1021/acsomega.3c03088
ACS Omega 2023, 8, 27488−27499